ACS OMEGA

http://pubs.acs.org/journal/acsodf

Article

Effect of Crystallinity on Water Vapor Sorption, Diffusion, and Permeation of PLA-Based Nanocomposites

Jon Trifol,* David Plackett, Peter Szabo, Anders Egede Daugaard, and Marco Giacinti Baschetti

Cite This: *ACS Omega* 2020, 5, 15362−15369

Read Online

ACCESS | Metrics & More | Article Recommendations | Supporting Information

ABSTRACT: The effects of crystalline morphology and presence of nanoparticles such as cellulose nanofibers (CNFs), organically modified nanoclay (C30B), or a combination of both on water vapor sorption and diffusion in polylactide (PLA) were evaluated by a quartz spring microbalance (QSM). It was found that the large spherulite size induced by high-temperature processing leads to an increase in water sorption and a substantial reduction of diffusion with increasing crystallinity. Contrarily, small-sized spherulites, arising after low-temperature processing during solvent-casting, showed a different behavior with a slight decrease in both water vapor sorption and diffusion with increasing crystallinity. These observations suggest that solvent-casting at low temperatures should not be used to predict the properties a material will show after industrial-scale processing. From the analysis of the nanocomposite materials, it was concluded that nanoparticles affected the material's properties not only by themselves but also by modifying the crystalline morphology. Interestingly, this led to CNF showing similar performance to C30B, decreasing water diffusivity (21 vs 27%) on isothermally crystallized materials despite its less favorable geometry. Additionally, the incorporation of 1 wt % CNF and C30B decreased water vapor transmission rate (WVTR) by 24% under an amorphous state but by 44% in a crystallized state, which makes hybrid CNF/C30B composites a promising food packaging material.

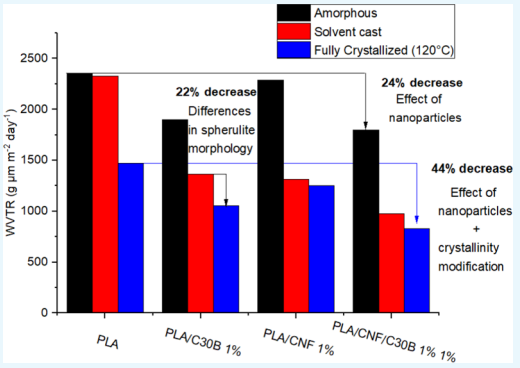

1. INTRODUCTION

The use of nondegradable petrochemical-based products for packaging applications is an issue of global concern and consequently substantial research efforts are being made to develop biobased and biodegradable materials such as polylactide (PLA) as substitutes. Unfortunately, in some respects, PLA has inferior characteristics when compared to the polymers currently used in packaging, especially regarding barrier properties.[1] To address this issue, PLA-based nanocomposites incorporating nanoclay,[2−4] nanocellulose,[5−8] or a combination of both[9,10] have been studied.

Interestingly, water vapor barrier properties of PLA/nanocellulose composites reported in the literature are quite variable. For CNC, cellulose nanocrystals, for example, Sanchez-Garcia and Lagaron[11] found a reduction of 82% in the WVTR (water vapor transmission rate) after addition of 3% w/w nanocrystalline cellulose (CNC) to PLA, while in contrast, Fortunati et al.[12] observed negligible reduction in the WVTR for PLA after addition of either 1% w/w or 5% w/w CNC. In another example, Espino-Perez and co-workers observed an almost three-fold increase in the WVTR when adding 15% nonmodified CNC to PLA.[8] In the case of cellulose nanofibers (CNFs), it was found that the incorporation of nonmodified CNF into PLA led to a significant increase in water sorption, which, however, was reduced when the CNF was acetylated.[13] Furthermore, Abdulkhani et al.[14] reported that the reinforcement of PLA with acetylated CNF led to small variations in the WVTR. In our previous work,[6] it was found that the addition of 1% of acetylated CNF to a PLA matrix led to a WVTR reduction of 46%.

The influence of crystallinity on water vapor interactions of PLA is also unclear and remains controversial.[15] In the traditional concept of a semicrystalline material, an increase in crystallinity usually results in decreasing water vapor sorption, since there is less material that can absorb water. However, it is generally accepted that water vapor sorption of PLA increases with crystallinity.[15] This is attributed to the de-densification of the amorphous phase during crystallization related to the creation of the RAF (rigid amorphous fraction). The latter shows an excess of free volume[16] where the gas can be absorbed.[15] In addition, investigation of crystallinity effects on water vapor transport becomes more difficult when nanoparticles are incorporated to PLA due to the nucleating agent behavior mentioned above.[17] The presence of nanoparticles affects the crystalline morphology of polymers and thus

Received: April 1, 2020
Accepted: June 5, 2020
Published: June 18, 2020

Table 1. Overview of the Materials Tested in This Work[25a]

	composition of the materials			
	PLA/CNF/C30B	X_c/MAF/RAF[b]	spherulite size[c,d]	thermal processing
PLA-SC	100/0/0	6/90/4	small	solvent-cast at 23 °C
PLA-AM	100/0/0	0/100/0		SC + quenching (amorphous)
PLA-FC	100/0/0	35/42/22	large, heterogeneous	SC + AM + 2 h at cryst. temp (120 °C)
PLA/C30B-SC	99/0/1	29/54/16	small	solvent-cast at 23 °C
PLA/C30B-AM	99/0/1	0/95/4		SC + quenching (amorphous)
PLA/C30B-FC	99/0/1	39/36/24	large	SC + AM + 2 h at cryst. temp (120 °C)
PLA/CNF-SC	99/1/0	34/41/25	large, partial	solvent-cast at 80 °C
PLA/CNF-AM	99/1/0	0/95/4		SC + quenching (amorphous)
PLA/CNF-FC	99/1/0	37/38/24	large	SC + AM + 2 h at cryst. temp (120 °C)
PLA/CNF/C30B-SC	98/1/1	35/35/28	large, partial	solvent-cast at 80 °C
PLA/CNF/C30B-AM	98/1/1	0/89/9		SC + quenching (amorphous)
PLA/CNF/C30B-FC	98/1/1	40/32/25	large	SC + AM + 2 h at cryst. temp (120 °C)

[a]SC stands for solvent-casting, AM for amorphous, and FC for fully crystallized. [b]X_c = degree of crystallinity, MAF = mobile amorphous fraction, RAF = rigid amorphous fraction. [c]Small size indicates submicron-sized spherulites, PLA-FC showing spherulites up to 100−120 μm, and PLA composites (both FC and SC around 20−30 μm). Heterogeneous indicates that the spherulite distribution was more diverse as what was observed for the composites where the nucleating agent behavior of the nanoparticles improved the distribution of the spherulites. [d]Partial indicates that the polarized optical microscopy of the films revealed dark regions between spherulites, which was not observed for FC materials.

generates the question as to whether any change in mass transport is due to the nanoparticle itself or due to the modification of the crystallinity.[8,18] The crystallinity severely impacts barrier properties of the pure polymer[19−21] and of the PLA-based composites.[22,23]

Following earlier results,[6,10,24,25] the present work focuses on the effect of different nanoparticles, CNF, C30B, and a combination of both, on water vapor sorption, diffusion, and permeation in PLA. The presence of nanofillers might affect water vapor permeability in a number of different ways: (i) by directly increasing the tortuous path inside the polymer, (ii) through variations in polymer chain mobility, which would influence penetrant diffusion in the matrix, and (iii) by means of crystallinity changes induced by the presence of nanofillers.

The aim of this study was to clarify the role of nanoparticles and thermal processing in the mass transport properties of PLA. In particular, water sorption and water diffusion of four different materials (a) PLA, (b) PLA/CNF 1%, (c) PLA/C30B 1%, and (d) PLA/CNF 1%/C30B 1% are analyzed after preparation under three different conditions: (a) amorphous state, (b) solvent-cast-induced crystallinity (low and high temperature), and (c) isothermal crystallization-induced crystalline morphology at the crystallization temperature of 120 °C.

2. RESULTS

2.1. Crystalline Morphology. As stated above, an investigation on the crystalline morphology of PLA and composites used in this study was carried out through polarized optical microscopy (POM), X-ray diffraction (XRD), and modulated dynamic scanning calorimetry (MDSC) and has already been published elsewhere;[25] however, a short summary is provided in Table 1.

Briefly, it was noted that the materials cast at a low temperature (23 °C) showed a small spherulite size (submicron scale), while materials processed at higher temperatures (cast at 80 °C or crystallized at 120 °C) showed larger spherulites (PLA-FC showed spherulites up to 100−120 μm while PLA composites, both FC and SC, around 20−30 μm) and a better distribution of spherulites in the polymer matrix. Additionally, the small spherulite size in composites was associated with reduced RAF.

It was also noteworthy that almost all of the crystallized materials (all SC and FC, except for PLA-SC) showed a similar degree of crystallinity (generally 34−40, 29% for the PLA/C30B-SC), and thus they were comparable to each other.

2.2. Water Diffusion. In Figure 1, the water diffusivity of the nanocomposites is shown as obtained from sorption experiments at 23 °C. Apart from absolute values, for the sake of clarity, the variation on water sorption on diffusion of the different materials referenced to PLA and amorphous materials is reported in the Supporting Information (Table S1). The values obtained for pure PLA are in agreement with previous reports[26,27] and, as in these cases, there are no significant variations in diffusivity with relative humidity (0−65%). In particular, as the standard deviation is below 10%, a constant value of diffusivity independent of water content can be assumed for all of the tested composites as well as the raw material. The same consideration can also be made for nanocomposites, as even in this case, no particular change in sorption kinetics is observed as a function of RH. Different diffusivity values were instead found for the different materials, which ranged from 1.05 to 4.05 × 10^{-8} cm^2/s, as reported in Figure 1A−C.

When investigating the impact of crystallinity on the water diffusivity of the materials (Figure 1A,C), it can be seen that all of the amorphous materials show a substantial decrease in diffusivity when crystallized at 120 °C, ranging from 49% of decrease of PLA (from PLA-AM to PLA-FC) to a 56.6% of decrease for PLA/CNF/C30B. This is attributed to the fact that the crystalline phase is virtually impermeable to water molecules, and thus increases the length of the path that molecules have to cross in the films (tortuosity), which leads to a substantial decrease in diffusion.

The most significant result can be observed in Figure 1B where data for solvent-cast samples are expressed. From this figure, composites showing a small spherulite size are associated with higher diffusivities when compared with composites showing large spherulite sizes. Specifically, PLA-SC and PLA/C30B-SC showed diffusivity values of 3.84 × 10^{-8} and 2.8 × 10^{-8} cm^2/s, respectively. These values contrast

https://dx.doi.org/10.1021/acsomega.0c01468
ACS Omega 2020, 5, 15362−15369

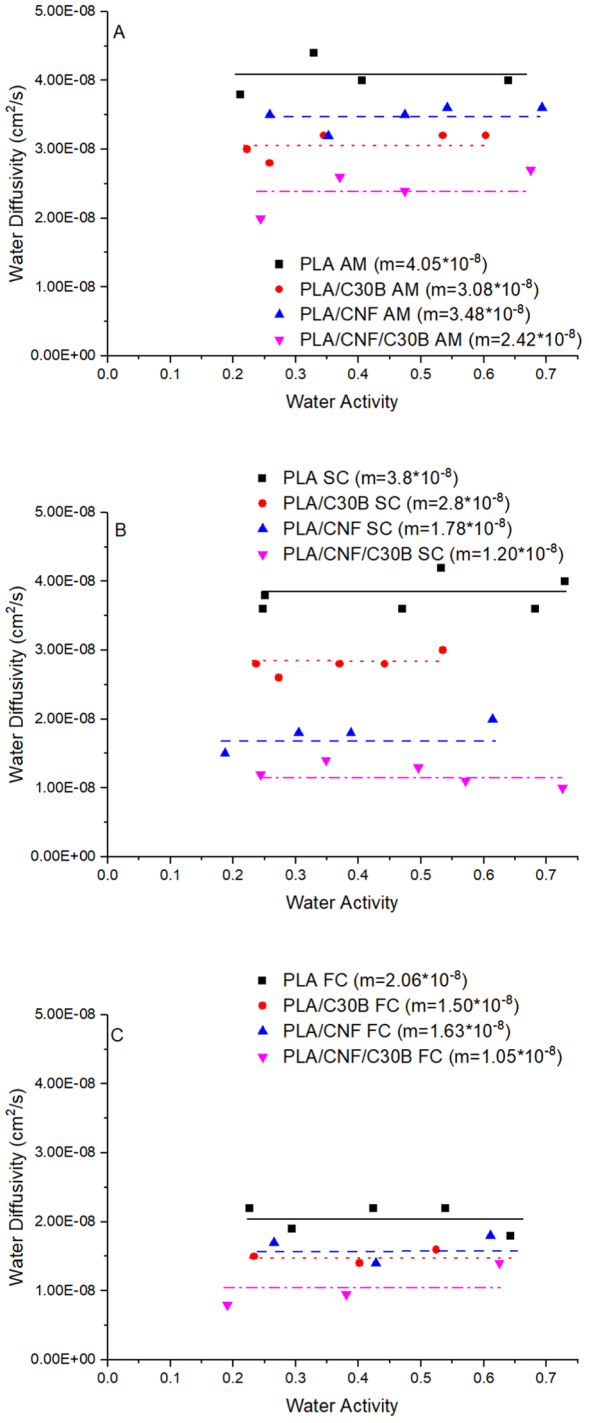

Figure 1. Diffusivity of PLA and its nanocomposites in different crystalline morphologies. (A) Fully amorphous (AM), (B) solvent-cast (SC), and (C) fully crystallized (FC) at 120 °C in isothermal crystallization. m = value of the average value (and therefore value of the diffusivity). Water activity is the partial pressure of the water in a substance divided by the partial pressure of water at the same conditions.

with PLA/C30B-FC, which showed a diffusivity of 1.5×10^{-8} cm^2/s. While for the case of PLA-SC, a substantially lower degree of crystallinity can be argued, PLA/C30B-SC, PLA/CNF-SC, and PLA/CNF/C30B-SC have similar degrees of crystallinity, meaning that the degree of crystallinity itself is unlikely to be the reason of change. However, it is noteworthy that the composites that were prepared by solvent-casting and that show large spherulite sizes (PLA/CNF-SC and PLA/CNF/C30B-SC) also show low diffusivity (1.78 and 1.2×10^{-8} cm^2/s), proving that it is the spherulite size and not the solvent-casting process that causes the high diffusivity. While this effect could also be attributed to variations on MAF, the decrease of diffusivity with increased particle size has been also reported by Gorrasi et al.,[28] which suggests that the spherulite size is indeed relevant for water diffusion. It can be speculated that a small spherulite size, meaning more spherulites, will lead to a better RAF distribution, and as a RAF has a higher free volume, the mass transport is likely to be faster in it. In other words, a water molecule will find a closer RAF region in a material with a small spherulite size, and thus it will migrate faster.

The incorporation of nanoparticles also causes a reduction in water diffusivity to a similar extent as crystallinity but at a substantially lower content (<2%). In particular, in the activity range observed, the effect seems to be additive. For example, for PLA/CNF/C30B-AM and FC samples with both 1% of CNF and 1% of C30B (2 wt % in total), a reduction of 40 and 49%, respectively, has been measured, which is approximately what is obtained by adding the reduction observed on PLA/CNF 1% and PLA/C30B 1%. Therefore, it can be concluded that the combination of nanocellulose and clay is an effective way to reduce diffusivity.

When comparing the performance of CNF and C30B, where composites show similar degrees of crystallinity, it can also be noted that CNF is slightly less efficient than nanocellulose in reducing the diffusivity. This is expected due to the fibrillar nature of CNF vs the two-dimensional (2D) shape of C30B, which can create longer tortuous paths inside the polymer. However, this effect is substantially reduced when composites are fully crystallized (14 vs 24% in the AM composites, 21 vs 27% in the FC composites).

This suggests that the presence of nanoparticles induces a crystalline structure that is more efficient in increasing the barrier properties. Interestingly, the incorporation of nanoparticles reduces the water diffusivity more in the fully crystallized state than in the amorphous state, which suggests that the incorporation of nanoparticles reduces water diffusivity not only by the nanoparticles themselves but also by modifying the crystallinity of the matrix. This might be due to a better spherulite distribution in the nanocomposites, resulting from the good nucleating behavior of CNF and C30B, whereas the different geometries of the nanoparticles appear to be less important.

In summary, it has been observed how small spherulites are not as efficient in reducing water diffusion as larger spherulites. Incorporation of a moderate amount of nanoparticles (1% of CNF and 1% of C30B) is as effective as ensuring full crystallization of the material in regard to reducing water diffusivity. Increasing the nanoparticle load in the material will further decrease the WVTR but not as noticeably as 1%.[10] Moreover, incorporation of nanoparticles reduces the water diffusion not only by the nanoparticles themselves but also by affecting the crystalline morphology, while the two types of nanoparticles (CNF and C30B) showed similar reduction in water diffusivity for fully crystallized materials.

2.3. Water Sorption. In Figure 2, the water sorption isotherm of the nanocomposites are shown. For the sake of clarity, Table S2 shows the variations of solubility coefficients, *S*, due to the incorporation of nanoparticles or crystallization.

https://dx.doi.org/10.1021/acsomega.0c01468
ACS Omega 2020, 5, 15362−15369

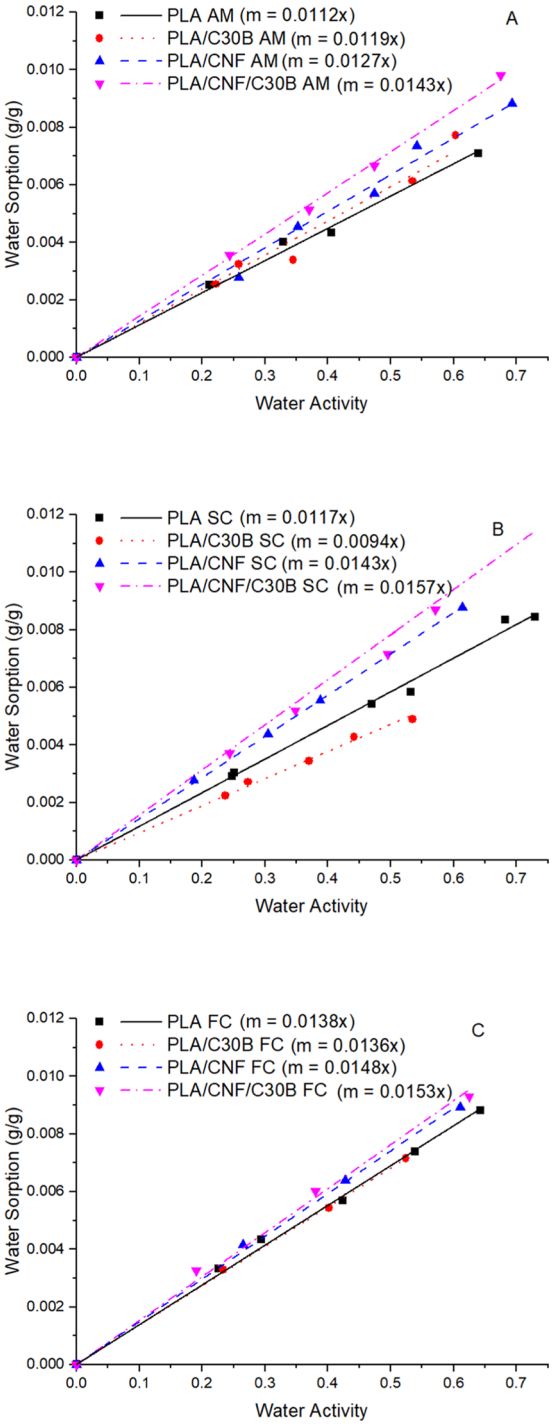

Figure 2. Water sorption of PLA and its nanocomposites at different crystalline morphologies. (A) Fully amorphous, (B) solvent-casting, and (C) fully crystallized (FC) at 120 °C in isothermal crystallization. Water activity is the partial pressure of the water in a substance divided by the partial pressure of water at the same conditions. m = slope of the curve (sorption coefficient).

All of the curves in Figure 2 present a linear increase in water sorption with activity, which is in line with previous studies on water sorption in PLA, although the overall value (0.0122) is slightly higher.[29−31] However, the reported differences can be attributed to the fact that different grades of PLA were used.

In general, and as reported in the literature, an increase in water sorption with increased crystallinity is observed, which is usually attributed to the de-densification of the MAF and/or to the fact that the RAF, which is higher for fully crystallized materials,[32] has a higher free volume.[16]

In line with the water diffusivity observations, there is a significantly different behavior between PLA and composites showing small- and large-sized spherulites with the former generally showing reduced water sorption. Indeed, PLA/C30B-SC (small spherulite size) shows the smallest water uptake of all of the composites (S = 0.0094), including the very same material crystallized at high temperature (PLA/C30B-FC; S = 0.0136) and the other solvent-cast materials (PLA/CNF-SC and PLA/CNF/C30B-SC). This confirms that the spherulite size plays a crucial role in water sorption.

Considering further the effect of the type of nanomaterial shown in Figure 2, it can be seen that the incorporation of nanoparticles in the polymer matrix also leads to increased water sorption. The increase of water sorption of the AM composites can be explained due to the sorption onto the nanoparticles themselves, which also explains the differences among CNF and C30B composites, as cellulose is more hydrophilic than the organically modified clay. Other explanations, which also involve the presence of the amorphous composite materials of a rigid amorphous fraction (RAF) at the interface between the polymer and the nanofiller, seem to have a secondary role as the RAF observed in PLA and PLA/C30B is similar (4%) (Table 1).

Interestingly, although FC materials show higher water sorption than AM ones, the water uptake in the nanocomposites is less affected by full crystallization than the neat PLA. As an example, the full crystallization of PLA increases the water sorption by 23%, while the full crystallization of PLA/C30B/CNF only increases water sorption by 7%. The presence of the nanomaterial, therefore, seems to counterbalance somewhat the increased sorption induced by PLA crystallization. Based on these results, although one of the main drawbacks of PLA is that water sorption can cause defects during processing, hybrid nanocomposites might present better processability due to lower water swelling.

2.4. Water Vapor Transmission. From the data on water vapor diffusion and water vapor sorption, the water vapor transmission rate (WVTR) at 23 °C and 50% could be estimated using eq 1. The results calculated by means of the quartz spring microbalance (QSM) are compared with the ones obtained in earlier studies[6,10] using the so-called cup method, as shown in Figure 3. Briefly, in the cup method, a recipient with a shape similar to a Petri dish is filled with a desiccating agent, and the test film is sealed to the open mouth and then hermetically closed. Thereafter, it is placed in a controlled environment (known temperature and humidity) and the mass increase of the cup is plotted against the time. As the cross section is known (from the geometry of the Petri dish), the WVTR can be calculated from the slope of the curve.

As can be seen in Figure 3, there is good agreement between the values calculated by both methods. Although the cup method provides slightly lower values than the QSM, the results are still comparable. Therefore, water permeation through PLA and composites can be concluded to be governed by the solution diffusion mechanism and the data can be used to discuss the expected behavior of the WVTR in other PLA composites.

Following this idea, Figure 4 compares the WVTR, as obtained using eq 1, for the different samples considered. Table S3 shows the % variation of the WVTR between

https://dx.doi.org/10.1021/acsomega.0c01468
ACS Omega 2020, 5, 15362−15369

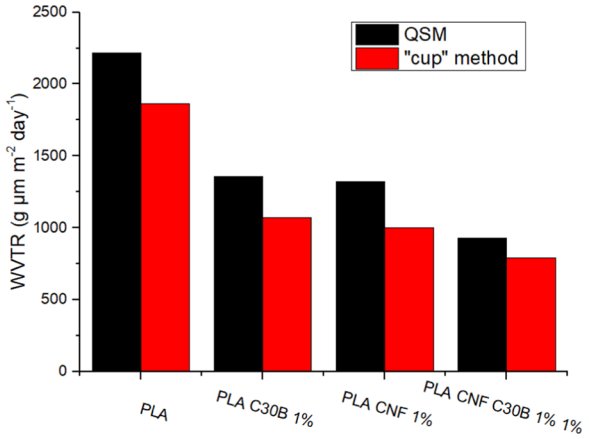

Figure 3. Comparison of the values of the WVTR obtained from the QSM and the so-called "cup method" of the solvent-cast (SC) materials.

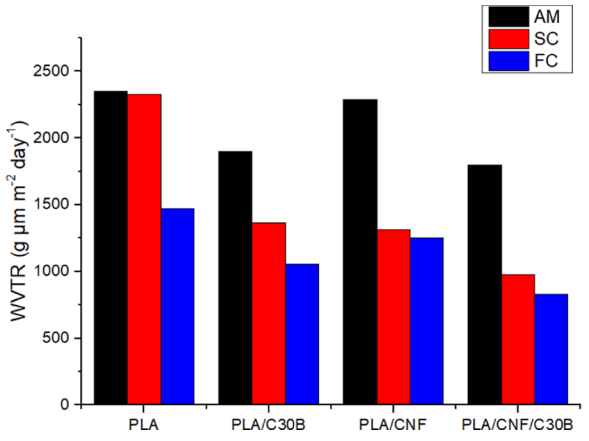

Figure 4. Water vapor transmission rate of PLA and its nanocomposites at different crystalline morphologies. Fully amorphous, solvent-casting, and isothermal crystallization.

materials due to crystallization or incorporation of nanoparticles. It can be observed that PLA/C30B-SC shows a substantial decrease in the WVTR when going from solvent-cast samples (small spherulite size) to fully crystallized samples (large spherulite size). This is in contrast with PLA/CNF and PLA/CNF/C30B, which show a similar WVTR in both SC and FC states, thus proving that small spherulite size is not as effective as large spherulite size in decreasing the WVTR. This explains the surprising results obtained in our earlier works where CNF was found to be a better reinforcing agent than C30B to improve barrier properties in solvent-cast materials and which now can be attributed to the different conditions used in the solvent-casting procedure.

For all materials, there is a substantial decrease in the WVTR when going from the amorphous composites to fully crystallized ones. Full crystallization was found to have an opposite effect on diffusivity and solubility. On one hand, full crystallization leads to a sharp decrease in water diffusion (Figure 1), while, on the other hand, it also leads to a minor increase in water sorption (Figure 2). However, as can be noted, the decrease in diffusivity is greater than the increase in sorption, therefore leading to a substantial decrease in the WVTR with increased crystallinity.

The impact of the nanoparticles on the WVTR is also very noticeable and similar to the full crystallization (the full crystallization and the addition of nanoparticles reduces the WVTR to a similar extent).

The influence of these parameters on permeability is not only related to the increase of diffusion pathways due to the addition of an impermeable filler but also due to their ability to promote polymer crystallization. Full crystallization of PLA causes a WVTR decrease of about 37%, whereas nanocomposite materials always show higher WVTR reductions, going from 45% for PLA/CNF and PLA/C30B up to 57% observed for PLA/CNF/C30B, which is the material showing the highest permeability decrease. Interestingly, among the different materials, the PLA/CNF/C30B nanocomposite, either in amorphous or in a fully crystallized state, shows the most significant decrease in terms of WVTR, making this hybrid nanocomposite a promising material to substitute petrol-based polymers for food packaging applications. Indeed, the fully crystallized hybrid composite (PLA/CNF/C30B-FC) shows a 65% decrease in the WVTR when compared with neat (amorphous) PLA.

3. CONCLUSIONS

In this work, the water sorption and water diffusion of neat PLA and PLA loaded with nanoclay and or nanocellulose were evaluated by means of a QSM. PLA, PLA/C30B 1 wt %, PLA/CNF 1 wt %, and PLA/CNF 1%/C30B 1% composites having three different crystalline morphologies obtained by (a) solvent-casting, (b) amorphous state, and (c) isothermal crystallization procedure were considered for the study.

The following observations were made:

- Spherulite size significantly affects the mass transport across the films. Small spherulites (achieved at low-temperature processing) are associated with a small decrease in water sorption and diffusion, whereas larger spherulites (achieved at higher-temperature processing) are associated with a substantial decrease in diffusion and a slight increase in water sorption. Therefore, alignment of thermal history with processing conditions is essential in evaluation and prediction of material properties.
- The incorporation of nanoparticles does not only decrease the WVTR and water diffusivity by the nanoparticles themselves but also by modifying the crystallinity of the polymer.
- C30B was found to be more efficient than CNF in decreasing WVTR and water diffusivity in the amorphous state, while both nanoparticles were found effective for fully crystallized PLA composites.
- For fully crystallized materials, the incorporation of only 1% of CNF or 1% of C30B in PLA had a similar impact on the water vapor transport.
- The hybrid PLA/CNF 1%/C30B 1% shows outstanding capabilities as a barrier material, as the fully crystallized material showed a 65% reduction of the WVTR when compared with neat PLA. In addition, among all composites, PLA/CNF 1%/C30B 1% is the one that showed a smaller increase in water sorption due to full crystallization (7% compared with 23% of PLA).

4. EXPERIMENTAL SECTION

4.1. Materials and Methods. L-Polylactide (Ingeo 2003D) was supplied by NatureWorks (Minnesota). The nanoclay used was Cloisite 30B (C30B), which is organically

https://dx.doi.org/10.1021/acsomega.0c01468
ACS Omega 2020, 5, 15362−15369

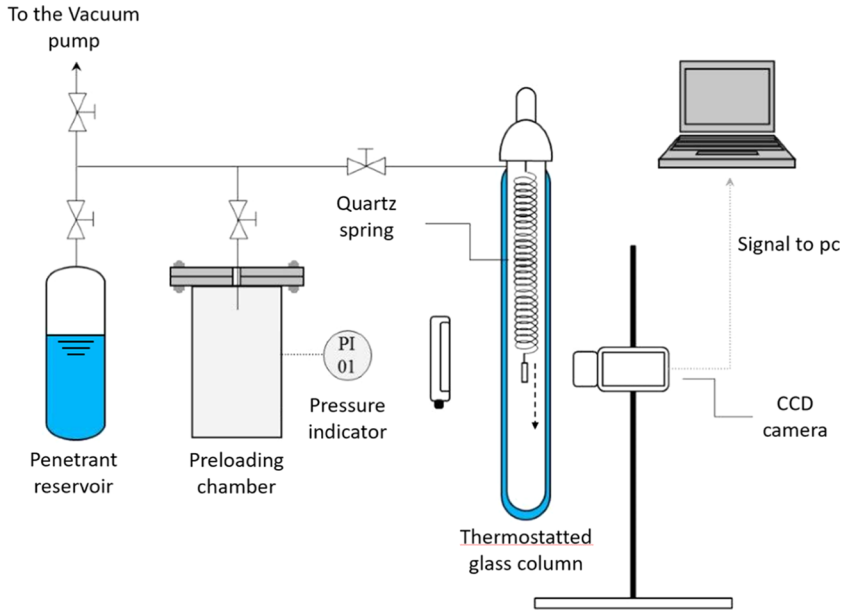

Figure 5. Schematics of the QSM that allows the monitoring of mass weight vs time.

modified with the addition of hydrophobic bis (2-hydroxyethyl)-methyl tallow alkyl ammonium cations.[33] The fully exfoliated platelets, with dimensions of approximately 400 × 300 × 1 nm,[34] are commercially available and well described in the literature.[35−37]

For the purposes of our experiments, cellulose nanofibers (CNFs) were extracted from sisal (*Agave sisalana*), which was kindly supplied by Export Sisal S.L (Las Palmas de Gran Canaria, Spain), according to a sequence of alkali-acetylation treatments followed by magnetic stirring. Details of the extraction procedure as well as of CNF characterization methods are available elsewhere.[24] CNF is reported to have a diameter of 27 ± 13 nm and a length of 658 ± 290 nm and with an acetylation degree of substitution (DS) in the order of 10%.

NaOH (>98%), sulfuric acid (95−97%), nitric acid (ACS reagent, 70%), acetic acid (99−100%), *N*,*N*-dimethylformamide (98%, ACS reagent), and dichloromethane (99, 8% chromasolv) were purchased from Sigma Aldrich and sodium chlorite (25% w/w in water) was obtained from Merck. All of the reagents were used as received.

4.1.1. Composite Preparation. PLA, PLA/C30B 1%, PLA/CNF 1%, and PLA/CNF 1%/C30B 1% were prepared as previously described.[6,10]

Briefly, neat PLA and nanofillers were dissolved/dispersed in a suitable solvent and then mixed in an appropriate ratio, cast into Teflon molds, and dried. In particular, dichloromethane (DCM) was used as a solvent for PLA and PLA/C30B, and the resulting samples were dried at 23 °C overnight. However, the use of DCM to prepare PLA/CNF composites led to a poor dispersion of the nanoparticles and thus dimethylformamide (DMF) was used for PLA/CNF and PLA/CNF/C30B, as it led to better dispersion of nanoparticles, and then dried at 80 °C overnight. Neat PLA and composite cast films showed a thickness of 80−90 μm with a standard deviation of less than 2.4 μm for each film (5 measurements per film). All of the compositions are expressed in wt % nanofiller by polymer weight.

4.1.2. Thermal Treatments. To obtain samples with different crystalline structures, various thermal pretreatments were applied, starting from the solvent-cast sample (SC). Amorphous (AM) samples were obtained by hot-pressing cast films at 170 °C for 5 min with 5 min of preheating at the same temperature followed by fast cooling. Briefly, the specimen was placed in between two thick aluminum foils, hot-pressed, and then fast cooled using cold water (5 °C). Then, the film was removed from the aluminum foils. Fully crystallized samples (FC) were obtained from the amorphous ones by maintaining samples at 120 °C for 2 h to achieve complete crystallization. An in-depth study on the crystallinity of the PLA and composites has been published elsewhere.[25]

For the sake of clarity and to give a quick reference during the data analysis and discussion, an overview of the composition, thermal history, and crystallinity of the materials investigated in the present study is provided in Table 1.

4.1.3. Mass Transport Properties. QSM (quartz spring microbalance) is an absorption-based instrument for the study of mass transport properties in films and membranes. This instrument does not directly provide permeability data but allows the diffusivity and the solubility of a test vapor into a material to be characterized. If a simple solution diffusion permeation mechanism[38] is applied, permeability can be obtained from sorption and diffusion values using the following equation

$$P = D^*S \quad (1)$$

where P is the permeability, D is the diffusivity, and S is the solubility coefficient, which is the increase in equilibrium concentration as a function of pressure.

The QSM (Figure 5) used in the present work is based on the use of a nonrotating quartz spring having a sensitivity of 1 mm/mg and a maximum load of 50 mg. The spring is mounted inside a water-jacketed glass column able to maintain the temperature within ±0.5 °C of the experimental set point, which was 23 °C in this case. Stainless steel tubes and valves allowed connections between the different parts of the apparatus and to the vacuum system consisting of a vacuum pump and a liquid nitrogen trap, which is used for sample

https://dx.doi.org/10.1021/acsomega.0c01468
ACS Omega 2020, 5, 15362−15369

degassing and evacuation of the test vapor. Samples were observed through a CCD Camera (Series 600 Smartimage sensors) manufactured by The DVT Corporation (Norcross, GA), and a strobe LED array illuminator, model IDRA-6, is located behind the glass column to achieve optimal illumination and maximum image contrast. The QSM could be used to measure weight differences in the order of 2 μg reliably. A complete description of the experimental setup can be found in the literature.[39]

Experiments were performed after complete dehydration of the film samples obtained by keeping the balance under vacuum until no weight change was observed. The vapor of the test solvent (water in this case) was then put in contact with the specimen at the desired pressure to start the experiments. As the water vapor started to penetrate into each sample, the mass of the latter, $m(t)$, increased with time and elongated the spring whose movements are recorded photographically. Once the sample had reached equilibrium at the working water activity, the total amount of water absorbed, m_∞, can be calculated from the elongation, and the diffusivity can be obtained from the plot of mass increase vs time through the use of appropriate models. In the case of a film of thickness L exposed on both sides to the penetrant, the following equation is considered valid[40]

$$\frac{m(t)}{m_\infty} = 1 - \frac{8}{\pi^2}\sum_{n=1}^{\infty}\frac{1}{(2n+1)^2}\exp\left[-(2n+1)^2\left(\frac{\pi}{L}\right)^2 Dt\right] \quad (2)$$

After equilibrium has been reached, the pressure inside the column can be increased further, and a new absorption step can be recorded at higher water activity. As long as the water sorption of PLA showed a linear behavior below ~70% RH,[41] at least three points were considered in this activity range to build the sorption isotherm and calculate the solubility coefficient, which is needed for permeability analysis as explained above.

■ ASSOCIATED CONTENT

Supporting Information

The Supporting Information is available free of charge at https://pubs.acs.org/doi/10.1021/acsomega.0c01468.

The supporting information contains three tables showing the percentage of variation between the samples to have a better overview on how crystallinity or presence of nanoparticles affect materials' properties (PDF)

■ AUTHOR INFORMATION

Corresponding Author

Jon Trifol − *Department of Chemical and Biochemical Engineering, Danish Polymer Centre, Technical University of Denmark, DK-2800 Lyngby, Denmark;* orcid.org/0000-0001-9447-1089; Email: jontrifol@gmail.com

Authors

David Plackett − *Faculty of Pharmaceutical Sciences, University of British Columbia, Vancouver, BC V6T 1Z3, Canada*

Peter Szabo − *Department of Chemical and Biochemical Engineering, Danish Polymer Centre, Technical University of Denmark, DK-2800 Lyngby, Denmark*

Anders Egede Daugaard − *Department of Chemical and Biochemical Engineering, Danish Polymer Centre, Technical University of Denmark, DK-2800 Lyngby, Denmark;* orcid.org/0000-0002-0627-6310

Marco Giacinti Baschetti − *Alma Mater Studiorum, Università degli Studi di Bologna Dipartimento di Ingegneria Civile, Chimica, Ambientale e dei Materiali (DICAM) Laboratori Ing., 40131 Bologna, Italy;* orcid.org/0000-0002-7327-1608

Complete contact information is available at: https://pubs.acs.org/10.1021/acsomega.0c01468

Notes

The authors declare no competing financial interest.

■ ACKNOWLEDGMENTS

The author is thankful to the FP7-People-2011, ITN Marie Curie International Training Network (ITN) for their financial support.

■ REFERENCES

(1) Zhang, J.; Tashiro, K.; Tsuji, H.; Domb, A. J. Disorder-to-Order Phase Transition and Multiple Melting Behavior of Poly(L-Lactide) Investigated by Simultaneous Measurements of WAXD and DSC. *Macromolecules* **2008**, *41*, 1352−1357.

(2) McLauchlin, A. R.; Thomas, N. L. Preparation and Characterization of Organoclays Based on an Amphoteric Surfactant. *J. Colloid Interface Sci.* **2008**, *321*, 39−43.

(3) Mohapatra, A. K.; Mohanty, S.; Nayak, S. K. Dynamic Mechanical and Thermal Properties of Polylactide-Layered Silicate Nanocomposites. *J. Thermoplast. Compos. Mater.* **2014**, *27*, 699−716.

(4) Najafi, N.; Heuzey, M. C.; Carreau, P. J. Polylactide (PLA)-Clay Nanocomposites Prepared by Melt Compounding in the Presence of a Chain Extender. *Compos. Sci. Technol.* **2012**, *72*, 608−615.

(5) Aulin, C.; Karabulut, E.; Tran, A.; Waïšgberg, L.; Lindström, T. Transparent Nanocellulosic Multilayer Thin Films on Polylactic Acid with Tunable Gas Barrier Properties. *ACS Appl. Mater. Interfaces* **2013**, *5*, 7352−7359.

(6) Trifol, J.; Plackett, D.; Sillard, C.; Hassager, O.; Daugaard, A. E.; Bras, J.; Szabo, P. A Comparison of Partially Acetylated Nanocellulose, Nanocrystalline Cellulose, and Nanoclay as Fillers for High-Performance Polylactide Nanocomposites *J. Appl. Polym. Sci.* 2016, *133* 43257, DOI: 10.1002/app.43257.

(7) Jonoobi, M.; Harun, J.; Mathew, A. P.; Oksman, K. Mechanical Properties of Cellulose Nanofiber (CNF) Reinforced Polylactic Acid (PLA) Prepared by Twin Screw Extrusion. *Compos. Sci. Technol.* **2010**, *70*, 1742−1747.

(8) Espino-Pérez, E.; Bras, J.; Ducruet, V.; Guinault, A.; Dufresne, A.; Domenek, S. Influence of Chemical Surface Modification of Cellulose Nanowhiskers on Thermal, Mechanical, and Barrier Properties of Poly(Lactide) Based Bionanocomposites. *Eur. Polym. J.* **2013**, *49*, 3144−3154.

(9) Hong, J.; Kim, D. S. Preparation and Physical Properties of Polylactide/Cellulose Nanowhisker/Nanoclay Composites. *Polym. Compos.* **2013**, *34*, 293−298.

(10) Trifol, J.; Plackett, D.; Sillard, C.; Szabo, P.; Bras, J.; Daugaard, A. E. Hybrid Poly(Lactic Acid)/Nanocellulose/Nanoclay Composites with Synergistically Enhanced Barrier Properties and Improved Thermomechanical Resistance. *Polym. Int.* **2016**, *65*, 988−995.

(11) Sanchez-Garcia, M. D.; Lagaron, J. M. On the Use of Plant Cellulose Nanowhiskers to Enhance the Barrier Properties of Polylactic Acid. *Cellulose* **2010**, *17*, 987−1004.

(12) Fortunati, E.; Peltzer, M.; Armentano, I.; Torre, L.; Jiménez, A.; Kenny, J. M. Effects of Modified Cellulose Nanocrystals on the Barrier and Migration Properties of PLA Nano-Biocomposites. *Carbohydr. Polym.* **2012**, *90*, 948−956.

(13) Tingaut, P.; Zimmermann, T.; Lopez-Suevos, F. Synthesis and Characterization of Bionanocomposites with Tunable Properties from Poly (Lactic Acid) and Acetylated Microfibrillated Cellulose. *Biomacromolecules* **2010**, *11*, 454−464.

(14) Abdulkhani, A.; Hosseinzadeh, J.; Ashori, A.; Dadashi, S.; Takzare, Z. Preparation and Characterization of Modified Cellulose Nanofibers Reinforced Polylactic Acid Nanocomposite. *Polym. Test.* **2014**, *35*, 73−79.
(15) Sangroniz, A.; Chaos, A.; Iriarte, M.; Del Río, J.; Sarasua, J. R.; Etxeberria, A. Influence of the Rigid Amorphous Fraction and Crystallinity on Polylactide Transport Properties. *Macromolecules* **2018**, *51*, 3923−3931.
(16) Lin, J.; Shenogin, S.; Nazarenko, S. Oxygen Solubility and Specific Volume of Rigid Amorphous Fraction in Semicrystalline Poly(Ethylene Terephthalate). *Polymer* **2002**, *43*, 4733−4743.
(17) Kose, R.; Kondo, T. Size Effects of Cellulose Nanofibers for Enhancing the Crystallization of Poly(Lactic Acid). *J. Appl. Polym. Sci.* **2013**, *128*, 1200−1205.
(18) Keshtkar, M.; Nofar, M.; Park, C. B.; Carreau, P. J. Extruded PLA/Clay Nanocomposite Foams Blown with Supercritical CO2. *Polymer* **2014**, *55*, 4077−4090.
(19) Cocca, M.; Lorenzo, M. L.; Di Malinconico, M.; Frezza, V. Influence of Crystal Polymorphism on Mechanical and Barrier Properties of Poly(l-Lactic Acid). *Eur. Polym. J.* **2011**, *47*, 1073−1080.
(20) Tsuji, H.; Okino, R.; Daimon, H.; Fujie, K. Water Vapor Permeability of Poly(Lactide)s: Effects of Molecular Characteristics and Crystallinity. *J. Appl. Polym. Sci.* **2006**, *99*, 2245−2252.
(21) Courgneau, C.; Domenek, S.; Lebossé, R.; Guinault, A.; Avérous, L.; Ducruet, V. Effect of Crystallization on Barrier Properties of Formulated Polylactide. *Polym. Int.* **2012**, *61*, 180−189.
(22) Picard, E.; Espuche, E.; Fulchiron, R. Effect of an Organo-Modified Montmorillonite on PLA Crystallization and Gas Barrier Properties. *Appl. Clay Sci.* **2011**, *53*, 58−65.
(23) Du, A.; Koo, D.; Ziegler, M.; Cairncross, R. A. The Effect of Heat Treatment on Water Sorption in Polylactide and Polylactide Composites via Changes in Glass-Transition Temperature and Crystallization Kinetics. *J. Polym. Sci., Part B: Polym. Phys.* **2011**, *49*, 873−881.
(24) Trifol, J.; Sillard, C.; Plackett, D.; Szabo, P.; Bras, J.; Daugaard, A. E. Chemically Extracted Nanocellulose from Sisal Fibres by a Simple and Industrially Relevant Process. *Cellulose* **2017**, *24*, 107−118.
(25) Trifol, J.; van Drongelen, M.; Clegg, F.; Plackett, D.; Szabo, P.; Daugaard, A. E. Impact of Thermal Processing or Solvent Casting upon Crystallization of PLA Nanocellulose and/or Nanoclay Composites. *J. Appl. Polym. Sci.* **2019**, *136*, No. 47486.
(26) Davis, E. M.; Minelli, M.; Giacinti Baschetti, M.; Elabd, Ya. Non-Fickian Diffusion of Water in Polylactide. *Ind. Eng. Chem. Res.* **2013**, *52*, 8664−8673.
(27) Gorrasi, G.; Anastasio, R.; Bassi, L.; Pantani, R. Barrier Properties of PLA to Water Vapour: Effect of Temperature and Morphology. *Macromol. Res.* **2013**, *21*, 1110−1117.
(28) Gorrasi, G.; Vittoria, V.; Murariu, M.; Da Silva Ferreira, A.; Alexandre, M.; Dubois, P. Effect of Filler Content and Size on Transport Properties of Water Vapor in PLA/Calcium Sulfate Composites. *Biomacromolecules* **2008**, *9*, 984−990.
(29) Koo, D.; Du, A.; Palmese, G. R.; Cairncross, R. A. Moisture Management of Polylactides: The Effect of Heat Treatment. *Polymer* **2012**, *53*, 1115−1123.
(30) Cairncross, R. A.; Becker, J. G.; Ramaswamy, S.; O'connor, R. Moisture Sorption, Transport, and Hydrolytic Degradation in Polylactide. *Appl. Biochem. Biotechnol.* **2006**, *131*, 774−785.
(31) Du, A.; Koo, D.; Theryo, G.; Hillmyer, M. A.; Cairncross, R. A. Water Transport and Clustering Behavior in Homopolymer and Graft Copolymer Polylactide. *J. Membr. Sci.* **2012**, *396*, 50−56.
(32) Wunderlich, B. Reversible Crystallization and the Rigid-Amorphous Phase in Semicrystalline Macromolecules. *Prog. Polym. Sci.* **2003**, *28*, 383−450.
(33) Bitinis, N.; Verdejo, R.; Maya, E. M.; Espuche, E.; Cassagnau, P.; Lopez-Manchado, M. A. Physicochemical Properties of Organo-clay Filled Polylactic Acid/Natural Rubber Blend Bionanocomposites. *Compos. Sci. Technol.* **2012**, *72*, 305−313.
(34) Ploehn, H. J.; Liu, C. Quantitative Analysis of Montmorillonite Platelet Size by Atomic Force Microscopy. *Ind. Eng. Chem. Res.* **2006**, *45*, 7025−7034.
(35) Mohapatra, A. K.; Mohanty, S.; Nayak, S. K. Poly(Lactic Acid) and Layered Silicate Nanocomposites Prepared by Melt Mixing: Thermomechanical and Morphological Properties. *Polym. Compos.* **2012**, *33*, 2095−2104.
(36) Katiyar, V.; Gerds, N.; Koch, C. B.; Risbo, J.; Hansen, H. C. B.; Plackett, D. Melt Processing of Poly(L-Lactic Acid) in the Presence of Organomodified Anionic or Cationic Clays. *J. Appl. Polym. Sci.* **2011**, *122*, 112−125.
(37) Rhim, J. W.; Hong, S. I.; Ha, C. S. Tensile, Water Vapor Barrier and Antimicrobial Properties of PLA/Nanoclay Composite Films. *LWT - Food Sci. Technol.* **2009**, *42*, 612−617.
(38) Wijmans, J. G.; Baker, R. W. The Solution-Diffusion Model: A Review. *J. Membr. Sci.* **1995**, *107*, 1−21.
(39) Piccinini, E.; Giacinti Baschetti, M.; Sarti, G. C. Use of an Automated Spring Balance for the Simultaneous Measurement of Sorption and Swelling in Polymeric Films. *J. Membr. Sci.* **2004**, *234*, 95−100.
(40) Cranck, J. *The Mathematics of Diffusion* 1975, DOI: 10.1016/0306-4549(77)90072-X.
(41) Davis, E. M.; Minelli, M.; Baschetti, M. G.; Sarti, G. C.; Elabd, Y. A. Nonequilibrium Sorption of Water in Polylactide. *Macromolecules* **2012**, *45*, 7486−7494.

https://dx.doi.org/10.1021/acsomega.0c01468
ACS Omega 2020, 5, 15362−15369